Iron oxide nanoparticles induce ferroptosis via the autophagic pathway by synergistic bundling with paclitaxel

QI NIE[1,2*], WENQING CHEN[1,2*], TIANMEI ZHANG[1], SHANGRONG YE[1], ZHONGYU REN[1], PENG ZHANG[1] and JIAN WEN[1,2]

[1]Guangxi Clinical Medical Research Center for Neurological Diseases, Affiliated Hospital of Guilin Medical University, Guilin, Guangxi 541001; [2]College of Pharmacy, Guilin Medical University, Guilin, Guangxi 541104, P.R. China

Received February 9, 2023; Accepted August 8, 2023

DOI: 10.3892/mmr.2023.13085

Abstract. In recent years, inhibiting tumor cell activity by triggering cell ferroptosis has become a research hotspot. The development of generic targeted nanotherapeutics might bring new ideas for non-invasive applications. Currently, the potential mechanism underlying the universal application of paclitaxel (PTX)-loaded iron oxide nanoparticles (IONP@PTX) to different types of tumors is unclear. The present study aimed to prepare IONP@PTX for targeted cancer therapy and further explore the potential mechanisms underlying the inhibitory effects of this material on the NCI-H446 human small cell lung cancer and brain M059K malignant glioblastoma cell lines. First, a CCK-8 assay was performed to determine cell viability, and then the combination index for evaluating drug combination interaction effect was evaluated. Intracellular reactive oxygen species (ROS) and lipid peroxidation levels were monitored using a DCFH-DA fluorescent probe and a C11-BODIPY™ fluorescent probe, respectively. Furthermore, western blotting assay was performed to determine the expression of autophagy- and iron death-related proteins. The experimental results showed that, compared with either IONP monotherapy, PTX monotherapy, or IONP + PTX, IONP@PTX exerted a synergistic effect on the viability of both cell types, with significantly increased total iron ion concentration, ROS levels and lipid peroxidation levels. IONP@PTX significantly increased the expression of autophagy-related proteins Beclin 1 and histone deacetylase 6 (HDAC6) in both cell lines (P<0.05), increased the expression of light chain 3 (LC3)-II/I in NCI-H446 cells (P<0.05) and decreased that of sequestosome1 (p62) in M059K cells (P<0.05). Moreover, the addition of rapamycin enhanced the IONP@PTX-induced the upregulation of Beclin 1, LC3-II/I and HDAC6 and the downregulation of mTORC1 protein in both cell lines (P<0.05). Moreover, rapamycin enhanced the IONP@PTX-induced downregulation of p62 protein in NCI-H446 cells (P<0.05), suggesting that IONP@PTX induces ferroptosis, most likely through autophagy. Collectively, the present findings show that IONP works synergistically with PTX to induce ferroptosis via the autophagic pathway.

Correspondence to: Professor Jian Wen, Guangxi Clinical Medical Research Center for Neurological Diseases, Affiliated Hospital of Guilin Medical University, 15 Lequn Road, Guilin, Guangxi 541001, P.R. China
E-mail: wenjian2400@163.com

*Contributed equally

Key words: iron oxide nanoparticle, paclitaxel, autophagy, ferroptosis, NCI-H446 cell, M059k cell

Introduction

Lung cancer is one of the most diagnosed types of cancer, the most common in China and the leading cause of cancer-related mortality worldwide, with an estimated 2 million new cases and 1.76 million deaths every year (1,2). Treatment options for small cell lung cancer (SCLC) are limited compared with other types of lung cancer and provide only a transient benefit for most patients (3). SCLC accounts for >15% of all lung cancers (4) and most cases are associated with smoking (5). SCLC is characterized by rapid disease progression and early widespread metastasis. Thus, 80-85% of patients have extensive-stage small cell lung cancer (ES-SCLC) at the time of initial diagnosis (6). For several years, the standard treatment for patients with ES-SCLC has been platinum-based combination chemotherapy, which has shown a survival benefit; however, despite favorable initial treatment effects, median survival has rarely exceeded 1 year (5). Most patients with ES-SCLC eventually die due to cancer recurrence, with only 10-20% of patients surviving longer than 2 years. Therefore, an in-depth search for drug targets is needed to develop effective combination therapies with minimal toxicity (5,7,8).

It is well known that the incidence of central nervous system tumors has a place in the statistics table of new cancers in China in 2022 (2). Glioblastoma (GBM) is the most common malignant primary brain tumor. GBM is classified by the World Health Organization as grade IV and the median survival of patients is only 8-18 months (8). Currently, treatment strategies for glioma include surgery, radiotherapy, chemotherapy, immunotherapy and targeted therapy (9,10). However, chemotherapeutic drugs have limited therapeutic effects when used alone (11). Therefore, combining chemotherapeutic drugs with

other carriers can overcome drug resistance and reduce their toxic side effects (10). For example, drug delivery systems such as polymeric micelles, liposomes and nanoparticles can all synergistically facilitate the passage of chemotherapy drugs across the blood-brain barrier to target the desired sites (10,12,13). The main obstacles to effective chemotherapy for glioma are drug resistance and toxicity. Accordingly, there is an urgent need for new drugs and drug delivery systems to alleviate these two challenges for clinical application.

The pioneering drug paclitaxel (PTX), extracted from *Taxus brevifolia*, is a chemical drug derived from natural plants approved by the U.S. Food and Drug Administration (14). There is considerable evidence to suggest that PTX is one of the most successful and widely used natural antitumor drugs in various tumors, including glioma (15-17) and lung cancer (18,19). Indeed, PTX selectively targets microtubules and causes cell cycle arrest at the G_2/M phase, inducing cytotoxic effects in a dose- and time-dependent manner. Recently, development of several innovative drug delivery formulations, such as nano-emulsions, nanosuspensions, nanoparticles, liposomes and polymeric micelles, have been used to enhance the targeted cell delivery of PTX (20-23). However, the biological characteristics of PTX, such as low bioavailability, poor water solubility and high incidence of toxicity (24), may affect its antitumor efficacy to a certain extent and cause allergies, gastrointestinal reactions, neurotoxicity and other adverse reactions. However, the aforementioned defects can be partially overcome with the help of nano-drug delivery systems (25).

Nanoparticles have been the topic of emerging research interest for their unique properties, including nanometer size, biocompatibility, large surface-to-volume ratio and easy surface modification (26). Traditional antitumor chemotherapy drugs, such as single and non-targeted drugs, are slowly being discontinued. For example, resistance to PTX monotherapy can occur in the treatment of prostate cancer, so docetaxel in combination with prednisone is now the recommended treatment for this disease (27). Since combination therapy has the synergistic effect of multiple drugs, which may act through different pathways, it can improve efficacy, reduce drug dosage and toxicity, and gradually replace the current cancer treatment strategy (28). Pulvirent *et al* (29) prepared a hybrid system including the iron oxide magnetic nanoparticles and a metal-organic framework subclass constituted by trivalent transition metals and bi- or tri-carboxylic ligands (MNPs@MIL) with a particle size of ≤50 nm, which retains the magnetic properties of the iron core and has the loading capacity of porous containing iron ions and MILs. Moreover, the same study showed that MNPs@MIL could carry, load and release a higher quantity of drugs. In the treatment of GBM with temozolomide, the MIL-modified MNPs were more endocytosed than the naked MNPs at all concentrations due to the capability of *in situ* PTX-loaded MNPs@MIL targeting to the nucleus and cytoplasm to produce antitumor effects, suggesting that the hybrid system is able to overcome the blood-brain barrier and target brain tumors. Recently, iron-based iron oxide nanoparticles (IONP) have been used in clinical practice (30). Drug-encapsulating nanoparticles can enter the blood system and reach specific tumor sites through their enhanced permeability and retention effect, which is defined as the process of extravasation of large molecules from leaky tumor vasculature and accumulation in the tumor tissue, continuously releasing the drug and eventually producing a significant inhibitory effect on tumor growth (31). It was shown that the PTX-loaded IONPs (IONP@PTX) synthesized by the present research group possess lower toxicity than PTX monotherapy, suggesting that IONP can reduce the toxicity of drugs and improve biosafety (32).

Autophagy is an evolutionarily conserved process for cellular degradation, yet it is frequently viewed in cancer biology as a double-edged sword with the twin functions of tumor development and tumor suppression (33). Autophagy-related protein (ATG), including Beclin 1 and mTOR, and autophagic pathways (i.e., the autophagy-lysosome pathway, ubiquitin-like protein system and mTOR signaling pathway) are involved in the pathological processes of cancer development (33,34). As one of the most crucial protein complexes in the creation of the autophagic pathway, Beclin1 is the first mammalian discovered tumor-associated ATG protein and it also plays a vital role in the production of autophagosomes as well as their expansion and maturation (35). mTOR1, a key autophagy regulator connected to endosomes and lysosome membranes, interacts with its effectors through phosphorylation and plays a role in the development of lysosomes as well as the suppression of the autophagic process (36,37). Sequestosome1 (p62) is a multifunctional adapter protein that regulates the accumulation of protein aggregates and autophagic clearance (38). Histone deacetylase 6 (HDAC6) is a member of class IIb HDAC family and it deacetylates microtubule proteins, resulting in microtubule depolymerization and disconnection of the autophagosomal lysosomal fusion pathway (39-41), thereby inhibiting a member of the ATG8 family, LC3, which is a marker of the autophagic process. Moreover, the state of cellular redox homeostasis has a significant impact on autophagy (42). A growing body of evidence suggests that excessive autophagy and lysosome activation may cause lipid peroxidation (LPD), promoting ferroptosis (43). Accordingly, it has also been recommended to induce autophagy-mediated cellular ferroptosis to kill cancer cells (43).

Ferroptosis is a nonapoptotic programmed cell death process that can eradicate tumors via reactive oxygen species (ROS) accumulation and iron-dependent pathways (44). In the acidic environment of tumors, Fe^{2+} and Fe^{3+} ions released from the iron-based nanoparticles participate in the Fenton reaction, which generates ROS and triggers LPD, eventually leading to excessive accumulation of iron ions and inducing tumor cell death by ferroptosis (45). In addition, ferroptosis can be triggered by inhibiting two types of small-molecule substances, namely system Xc-mediated cystine uptake and glutathione peroxidase 4 (GPX4) (46). On the other hand, depleting L-cysteine (Cys) can also sensitize cells to ferroptosis through direct or indirect cysteine dioxygenase type 1-mediated metabolism of Cys, thereby reducing glutathione (GSH) expression (46). In a previous study, the nuclear factor erythroid 2-related factor 2 (Nrf2) was demonstrated to be involved in ferroptosis regulation and the treatment of neurodegenerative diseases (47).

PTX is one of the most frequently prescribed medications in Japanese clinical practice to treat recurrent SCLC and the efficacy of nanoparticle albumin-bound (nab)-PTX monotherapy might be moderate for heavily treated, relapsed

SCLC patients (19). Several studies reported the use of PTX combined with carboplatin, gemcitabine or albumin-bound PTX nanoparticles for the treatment of metastatic or recurrent SCLC, indicating that PTX as second-line chemotherapy is a good choice for the treatment of patients with SCLC (48-50). After nano-microsized modification, PTX is an ideal drug for the treatment of SCLC due to its improved therapeutic efficiency and diminished side effects. Based on nanoformulations, PTX can improve drug solubility, targeted activity, attenuate side effects after excisional surgery and effectively inhibit the growth of GBM cells (51,52). Accumulating evidence suggests that PTX is a broad-spectrum antitumor drug and has been used against human cancers, including glioma (25,53-55). For instance, it has recently been reported that an *in situ* targeted nanoparticle-hydrogel hybrid system modified with PTX could enhance the therapeutic effect of chemo-immunotherapy on residual infiltrative glioma (56). Nonetheless, to the best of our knowledge, there are only a few reports on the effects of IONP@PTX on NCI-H446 and M059K cells. Therefore, elucidating the possible mechanisms underlying the treatment of IONP@PTX *in vitro* is of profound importance for the development of universal application targeted therapies against SCLC and GBM, which may provide new therapeutic ideas for clinical applications, particularly for non-invasive therapeutic approaches. On this basis, the present study focused on the possible synergistic effect of IONP@PTX on SCLC H446 and GBM M059K cells and further explored its potential mechanisms.

Materials and methods

Preparation of IONP@PTX. High-temperature pyrolysis was used to create oleic acid-coated IONP. Briefly, 0.7 g $Fe(acac)_3$ (Shanghai Aladdin Chemical Reagent Co., Ltd.), 3.1 ml oleic acid (Shanghai Aladdin Chemical Reagent Co., Ltd), and 0.9 ml oleylamine (Shanghai Aladdin Chemical Reagent Co., Ltd.) were dissolved in 20 ml benzyl ether (Shanghai Aladdin Chemical Reagent Co., Ltd.), preheated at 220˚C for 1 h and subsequently heated to 280-300˚C for 30 h under the protection of nitrogen. After cooling to room temperature, the mixture was transferred into 30 ml anhydrous ethanol to collect the oleic acid-coated IONP through magnetic separation and then dissolved in 10 ml chloroform. Subsequently, 150 mg 1,2-distearoyl-sn-glycero-3-phosphoethanolamine-N-[amino (polyethylene glycol)-2000] (DSPE-PEG 2000) (Shanghai Advanced Vehicle Technology, Co., Ltd.) and 5.5 mg PTX (Shanghai Aladdin Chemical Reagent Co., Ltd) were weighed and put into an eggplant-shaped container with 5 ml trichloromethane. Then, 11 mg oleic acid-coated IONP and 11 ml distilled water were added and mixed ultrasonically to make an emulsion, as previously described (32). Thereafter, the suspension was concentrated through gentle solvent evaporation using a rotavapor for 50 min in a 70˚C water bath until the product was clear and transparent without visible bubbles, as previously described (32). Finally, the mixed emulsion was transferred to an ultrafiltration tube (0.5 ml, 3 kDa) to separate and purify the IONP@PTX, as previously described (32).

Drug loading capacity. Briefly, 1 mg/ml IONP@PTX solution was aspirated and diluted 25 times to measure the peak area by high performance liquid chromatography at 227 nm, as descried in our previous study (32). The peak area, which was 293522, was substituted into the standard curve y=26736 x + 1154.9, R^2=0.9987, to obtain the concentration and then to calculate the loading capacity of PTX/mg (iron concentration) solution using the following formula: Loading capacity=concentration x dilution x volume.

Cell culture. Human SCLC NCI-H446 cells and human GBM M059K brain malignant cells were obtained from Jiangsu KGI Biotechnology Co., Ltd. NCI-H446 cells were cultured in 90% RPMI-1640 (Gibco; Thermo Fisher Scientific, Inc.) supplemented with 10% FBS (Gibco; Thermo Fisher Scientific, Inc.), 100 U/ml penicillin and 100 μg/ml streptomycin (P/S). Similarly, M059K cells were cultured in 90% DMEM/F12 (Gibco; Thermo Fisher Scientific, Inc.) supplemented with 10% FBS and P/S (Beijing Solarbio Science & Technology Co., Ltd.). Both cell lines were placed in an incubator at 37˚C with 5% CO_2 and saturated humidity (Thermo Fisher Scientific, Inc.).

Cell viability. Following digestion with 0.25% EDTA-free trypsin (cat. no. C0205; Shanghai Biyuntian Biotechnology Co., Ltd.), the NCI-H446 and M059K cells were separately counted and adjusted to a cell suspension of $5x10^4$ cells/ml. Subsequently, 100 μl cell suspension was transferred to each well of a 96-well cell culture plate and cultured for 24 h. After discarding the old culture medium, 100 μl NCI-H446 cells (or M059K cells) were treated with IONP (0.7 μg/ml), PTX (0.3 μg/ml), IONP (0.7 μg/ml) + PTX (0.3 μg/ml), and IONP@PTX (1.0 μg/ml) at 37˚C for 24 h. Simultaneously, untreated cells were set as a negative control. Thereafter, 10 μl Cell Counting Kit-8 solution (cat. no. KGA317; Nanjing KeyGen Biotech Co., Ltd.) was added to each well and incubated for another 2 h. After shaking gently for 10 min, the optical density (OD) of each well was detected at 450 nm on a microplate reader (BioTek ELx800; BioTek) and cell growth inhibitory rate was calculated using the formula: Inhibitory rate (%)=[(OD of control group-OD of experimental group)/(OD of control group-OD of blank group)] x100. As shown in a previous study (57), the calculation formula of drug interaction was calculated using the following formula: combination index=$E_{a+b}/(E_a + E_b-E_a \times E_b)$, where a and b are any two treatments, E_{a+b} is the inhibitory rate of the combined a and b treatments, and E_a and E_b are separately the inhibitory rates of a and b. A combination index between 0.85 and 1.15 shows an additive effect and its value >1.15 shows synergistic interactions.

Detection of iron ion. Total iron ion concentration was quantified with an Iron Colorimetric Assay Kit (cat. no. E1042; Applygen Technologies, Inc.). Under the premise of the above grouping, the autophagy promoter rapamycin (50 nM; MedChemExpress) was separately added to each group, namely IONP (0.7 μg/ml) + rapamycin (50 nM), PTX (0.3 μg/ml) + rapamycin (50 nM), IONP (0.7 μg/ml) + PTX (0.3 μg/ml) + rapamycin (50 nM), IONP@PTX (1.0 μg/ml) + rapamycin (50 nM), and untreated cells (negative control). Following the aforementioned treatment of NCI-H446 and M059K cells, both cells were separately washed twice with cold PBS (cat.

no. C0221A; Shanghai Biyuntian Biotechnology Co., Ltd.) and lysed with 200 μl lysis buffer per well on a shaker for 2 h. In 100 μl cell lysate, 100 μl PBS and 4.5% potassium permanganate mixture were added, mixed gently, incubated at 60˚C for 1 h and then cooled to room temperature. Subsequently, 30 μl Iron ion detection agent was added, mixed gently and incubated at room temperature for another 30 min. Finally, all liquid was placed into a 96-well plate and absorbance was measured at 550 nm on a microplate reader (BioTek ELx800; BioTek).

Detection of intracellular ROS. Diacetyldichlorofluorescein (DCFH-DA) fluorescent probe (cat. no. KGT010-1; Jiangsu Kaiji Biotechnology Co., Ltd.) was used to detect the level of intracellular ROS. In brief, NCI-H446 and M059K cells were separately prepared for a cell suspension at a density of $5x10^5$ cells/ml, plated into a 6-well plate for 24 h and then treated as aforementioned. Meanwhile, untreated cells were set as a negative control. The cells were digested with 0.25% EDTA-free trypsin, collected and washed with PBS three times and centrifuged at 110 x g for 5 min at 24˚C. Thereafter, $1x10^6$ cells/ml were suspended in DCFH-DA (1:1,000) at a final concentration of 10 μmol/l, routinely cultured at 37˚C for 20 min and mixed at 3-5 min intervals. Finally, the stained cells were washed with serum-free RPMI-1640 three times to fully remove the free DCFH-DA and then intracellular ROS was detected (excitation wavelength, 488 nm; Emission wavelength, 530 nm) using flow cytometry (CytoFLEX; Beckman Coulter, Inc.).

Detection of lipid peroxidation. Intracellular LPD was detected using the C11-BODIPYTM (cat. no. D3861; Thermo Fisher Scientific, Inc.) fluorescent probe. Briefly, the pretreated NCI-H446 and M059K cells were separately washed three times with PBS at 110 x g for 5 min at 24˚C, collected, and adjusted to $1x10^6$ cells/ml. The cells were suspended in the 1:1,000 diluted C11-BODIPYTM at a final concentration of 10 μmol/l, routinely cultured at 37˚C for 20 min, and mixed at 3-5 min intervals. After washing the stained cells three times with serum-free RPMI-1640 to fully remove the free C11-BODIPYTM, the intracellular LPD was finally detected using flow cytometry (CytoFLEX; Beckman Coulter, Inc.).

Western blotting assay. The pretreated NCI-H446 cells and M059K cells were separately collected to extract the protein from the cell lysate following 15 min of centrifugation at 21,912 x g at 4˚C, and the protein concentration was determined using a BCA protein content detection kit (cat. no. KGA902; Nanjing KeyGen Biotech Co., Ltd.). First, identical amounts of protein (20 μg/lane) were separated on 10% gels using SDS-PAGE, transferred to PVDF membranes and blocked with fresh 5% nonfat dry milk at room temperature for 2 h. The membrane was incubated with diluted primary antibodies, including rabbit anti-P62 (1:1,000; cat. no. ab91526; Abcam), Nrf2 (1:5,000; cat. no. ab62352; Abcam), GPX4 (1:2,000; cat. no. ab123066; Abcam), mammalian target of rapamycin complex 1 (mTORC1) (1:2,000; cat. no. ab40768; Abcam), LC3II/I (1:2,000; cat. no. ab192890; Abcam), Beclin1 (1:1,000; cat. no. ab62557; Abcam), HDAC6 (1:10,000; cat. no. ab133493; Abcam), and GAPDH (1:5,000; cat. no. KGAA002; Nanjing KeyGen Biotech Co., Ltd.). After washing with Tris-buffered saline-Tween (TBST) three times, the membrane was subsequently incubated with the Goat Anti-Rabbit IgG/HRP antibody (1:10,000; cat. no. KGAA002; Nanjing KeyGen Biotech Co., Ltd.) for 1 h at room temperature. Following washing with TBST again, the blots were developed using a chemiluminescence detection system (ECL Luminata Crescendo; cat. no. WBLUR0500; MilliporeSigma).

Table I. Q value of drug interaction in NCI-H446 cells and M059K cells.

Group	Cell growth inhibitory rate, %	Q value
NCI-H446 cells		
IONP	1.66±0.51	-
PTX	40.24±0.79	-
IONP + PTX	41.70±0.99	0.953
IONP@PTX	64.24±0.53	1.46
M059K cells		
IONP	2.49±1.72	-
PTX	46.93±1.34	-
IONP + PTX	45.88±2.23	1.03
IONP@PTX	70.90±2.68	1.59

IONP, iron oxide nanoparticles; PTX, paclitaxel.

Statistical analysis. GraphPad Prism 8.0.1 software (GraphPad Software; Dotmatics) was used for statistical analysis. All data in this study are based on at least three replicated experiments. All data are expressed as the mean ± standard deviation and analyzed using either one-way ANOVA or two-way ANOVA followed by Tukey's post hoc test among groups. $P<0.05$ was considered to indicate a statistically significant difference.

Results

Characterization of IONP@PTX. As reported in our previous study (32), the synthesized IONP@PTX was uniformly distributed, with a core particle size of 10 nm, a hydrated particle size of 36.18±11.76 nm, a zeta potential of-29±7.65 mV and a drug loading value of 273.5 μg/mg (iron concentration) solution.

Effects of IONP@PTX on the cell growth inhibitory rates. After 24 h of treatment with IONP, PTX, IONP + PTX, and IONP@PTX, the cell growth inhibitory rates, both for NCI-H446 and M059K cells, were significantly higher in the IONP@PTX group, compared with those in the PTX monotherapy group or the IONP + PTX group ($P<0.001$); however, there was no significant difference between the PTX monotherapy group and the IONP + PTX group ($P>0.05$; Fig. 1A and B).

According to the cell inhibition rate calculation, the cell growth inhibitory rate of IONP + PTX was 41.70±0.99% in NCI-H446 cells and 45.88±2.23% in M059K cells, and the combination index was 0.953 in NCI-H446 cells and 1.03 in M059K cells, which is between 0.85 and 1.15, therefore

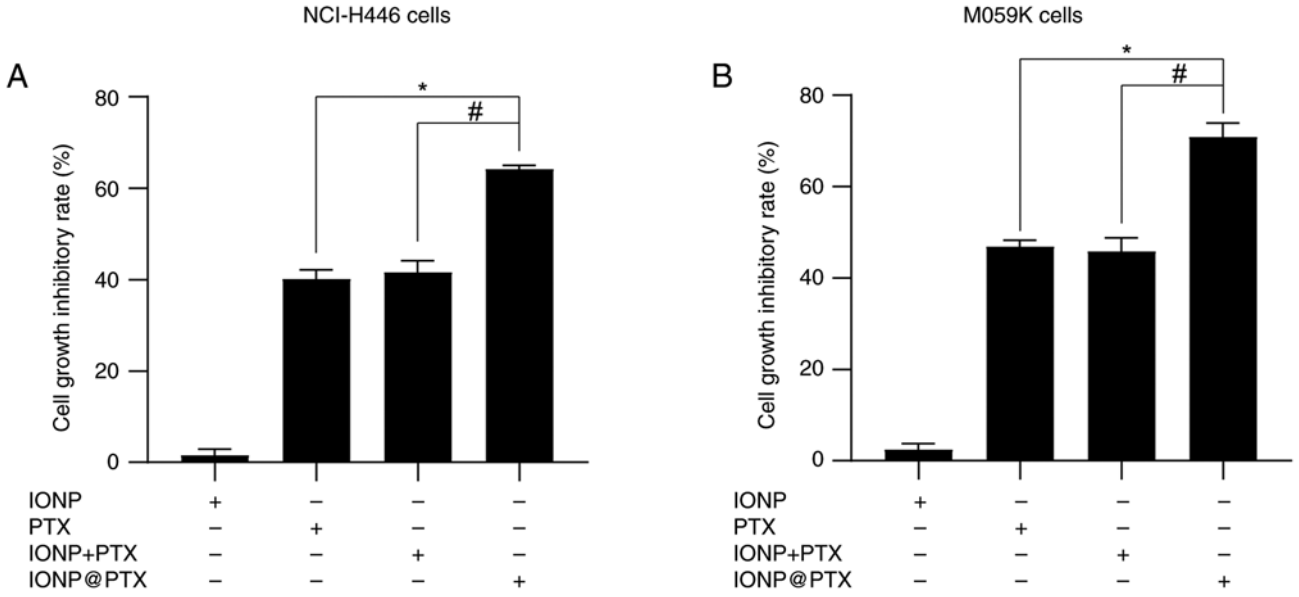

Figure 1. NCI-H446 and M059K cell growth inhibitory rates after 24 h treatment with different drugs. (A) NCI-H446 cell growth inhibitory rates. (B) M059K cell growth inhibitory rates. *P<0.05 vs. PTX group. #P<0.05 vs. IONP + PTX group. Data were obtained from three independent repeated experiments. IONP, iron oxide nanoparticles; PTX, paclitaxel.

showing an additive effect. However, the cell growth inhibitory rate of IONP@PTX was 64.24±0.53% in NCI-H446 cells and 70.90±2.68% in M059K cells, and the combination index was 1.46 in NCI-H446 cells and 1.59 in M059K cells, which is >1.15, therefore showing synergistic interactions. These results in H446 and MO59K cells indicate that IONP@PTX significantly exerts a synergistic effect on cell viability, compared with either PTX monotherapy or IONP + PTX (Fig. 1; Table I).

Effects of IONP@PTX on the induction of ferroptosis in NCI-H446 and M059K cells. After 24 h of co-incubation of NCI-H446 cells with IONP, PTX, IONP + PTX, and IONP@PTX, the total iron ion content, ROS and LPD levels measured using DCFH-DA and C11-BODIPY™, respectively, were significantly higher in the IONP@PTX group than those in the other groups (all P<0.05; Fig. 2A-E). However, the levels of ferroptosis-related protein Nrf2 in the IONP@PTX group were slightly lower than those in the other groups, while the levels of GPX4 were slightly lower in the IONP@PTX group than those in the IONP + PTX group but there were no significant differences among them (P>0.05; Fig. 3A, G and H).

Similar results were also obtained in M059K cells in terms of total iron ion content, ROS and LPD levels (P<0.05; Fig. 4A-E). In addition, a significantly lower expression of ferroptosis-related protein GPX4 was measured in the IONP@PTX group compared with that in the IONP + PTX group (P<0.05). In addition, the protein expression of Nrf2 was slightly lower but did not reach a statistical significance (P>0.05; Fig. 5A, G and H). These results were consistent in both cell lines following incubation with or without rapamycin (P<0.05; Figs. 3A, G and H, and 5A, G and H). Collectively, IONP@PTX significantly increases the levels of ROS, ferric ions and LPD in both cell lines. Moreover, the synergistic effect of IONP@PTX can be enhanced by addition of rapamycin, indicating that the autophagy promoter rapamycin enhances the IONP@PTX-induced cellular ferroptosis.

Effects of IONP@PTX on the induction of autophagy in NCI-H446 and M059K cells. Compared with PTX, IONP@PTX significantly increased the expression of autophagy-related proteins Beclin 1, LC3-II/I and HDAC6 (P<0.05) in NCI-H446 cells; however, there were no significant differences in the p62 and mTORC1 expression. Notably, compared with IONP + PTX, IONP@PTX significantly increased the expression of autophagy-associated proteins LC3 and HDAC6 in NCI-H446 cells (P<0.05; Fig. 3A-F).

Compared with PTX, IONP@PTX significantly increased the expression of autophagy-related proteins Beclin 1, HDAC6 and significantly decreased the expression of p62 protein (P<0.05) in M059K cells; however, there were no significant differences in the LC3-II/I and mTORC1 expression (P>0.05). Notably, compared with the IONP + PTX, IONP@PTX significantly increased the expression of autophagy-associated HDAC6 and significantly decreased the expression of p62 protein in M059K cells (P<0.05; Fig. 5A-F).

Furthermore, additional rapamycin enhanced the IONP@PTX-induced the upregulation of Beclin1, LC3 and HDAC6, as well as the downregulation of mTORC1 in NCI-H446 and M059K cells (P<0.05). Moreover, rapamycin enhanced the IONP@PTX-induced downregulation of p62 protein in NCI-H446 cells (P<0.05; Figs. 3A-F and 5A-F). These results indicate that the autophagic signaling pathway may be involved in the IONP@PTX-induced ferroptosis of H446 and M059K cells.

Discussion

It has been demonstrated in our previous study that IONP is effective for the induction of ferroptosis in GBM U251 cells (58) and IONP can effectively synergize with chemotherapeutic drugs against tumors via ferroptosis (59). It can therefore be inferred that IONP is expected to be a carrier for effectively transporting PTX and synergizing PTX against cancer cells.

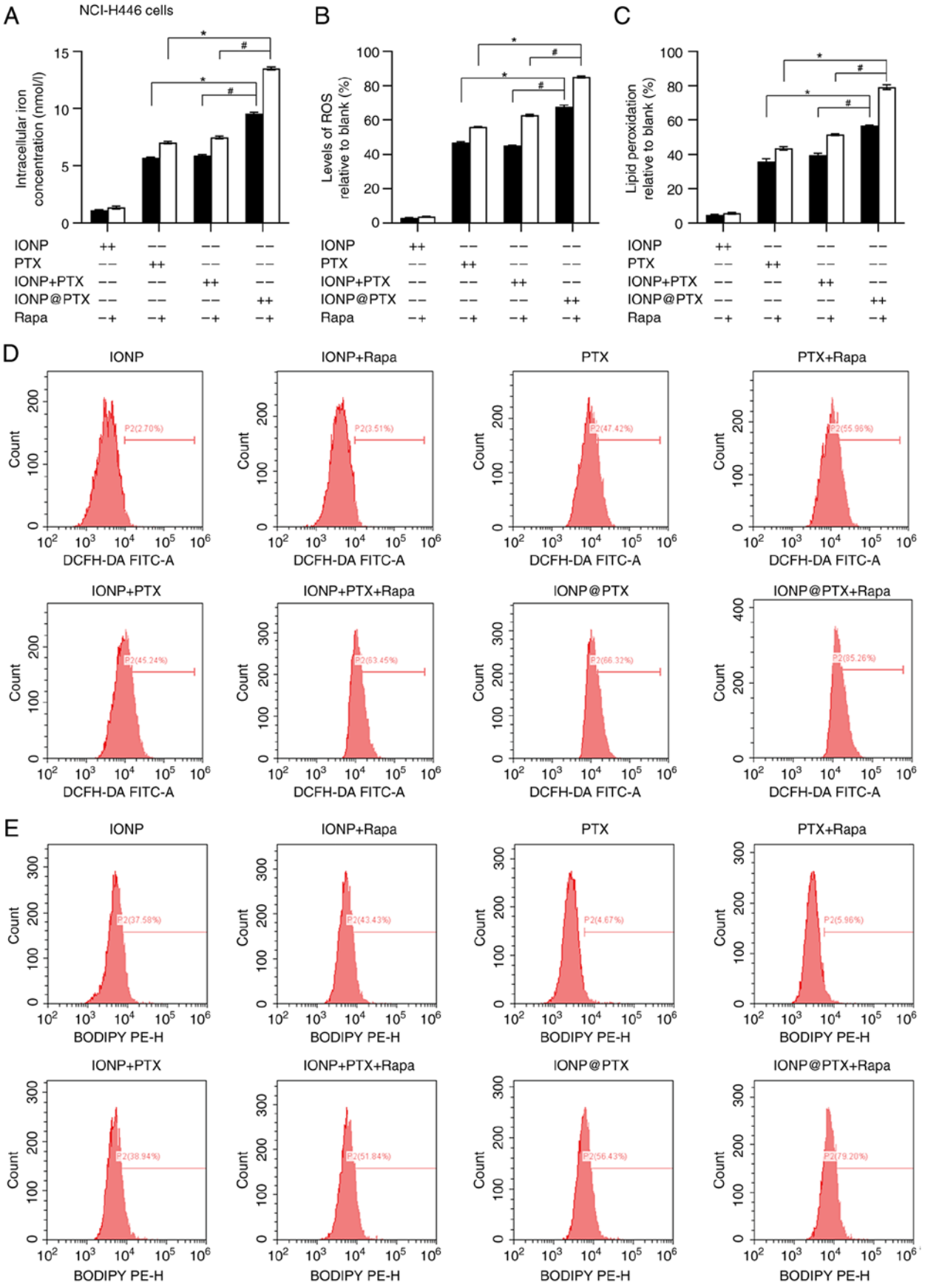

Figure 2. Changes in biochemical indices related to ferroptosis in NCI-H446 cells following treatment with IONP@PTX. (A) Intracellular iron concentration in NCI-H446 cells following treatment with or without 50 nmol/l rapamycin for 24 h. (B) Relative levels of ROS in NCI-H446 cells following treatment with or without 50 nmol/l rapamycin for 24 h. (C) Relative levels of lipid peroxidation in NCI-H446 cells following treatment with or without 50 nmol/l rapamycin for 24 h. (D) Flow cytometry analysis using DCFH-DA fluorescent probe to measure the intracellular ROS content. (E) Flow cytometry analysis using C11-BODIPY fluorescent probe to measure intracellular lipid peroxidation content. *P<0.05 vs. PTX group. #P<0.05 vs. IONP + PTX group. Data were obtained from three independent repeated experiments. IONP, iron oxide nanoparticles; PTX, paclitaxel; ROS, reactive oxygen species.

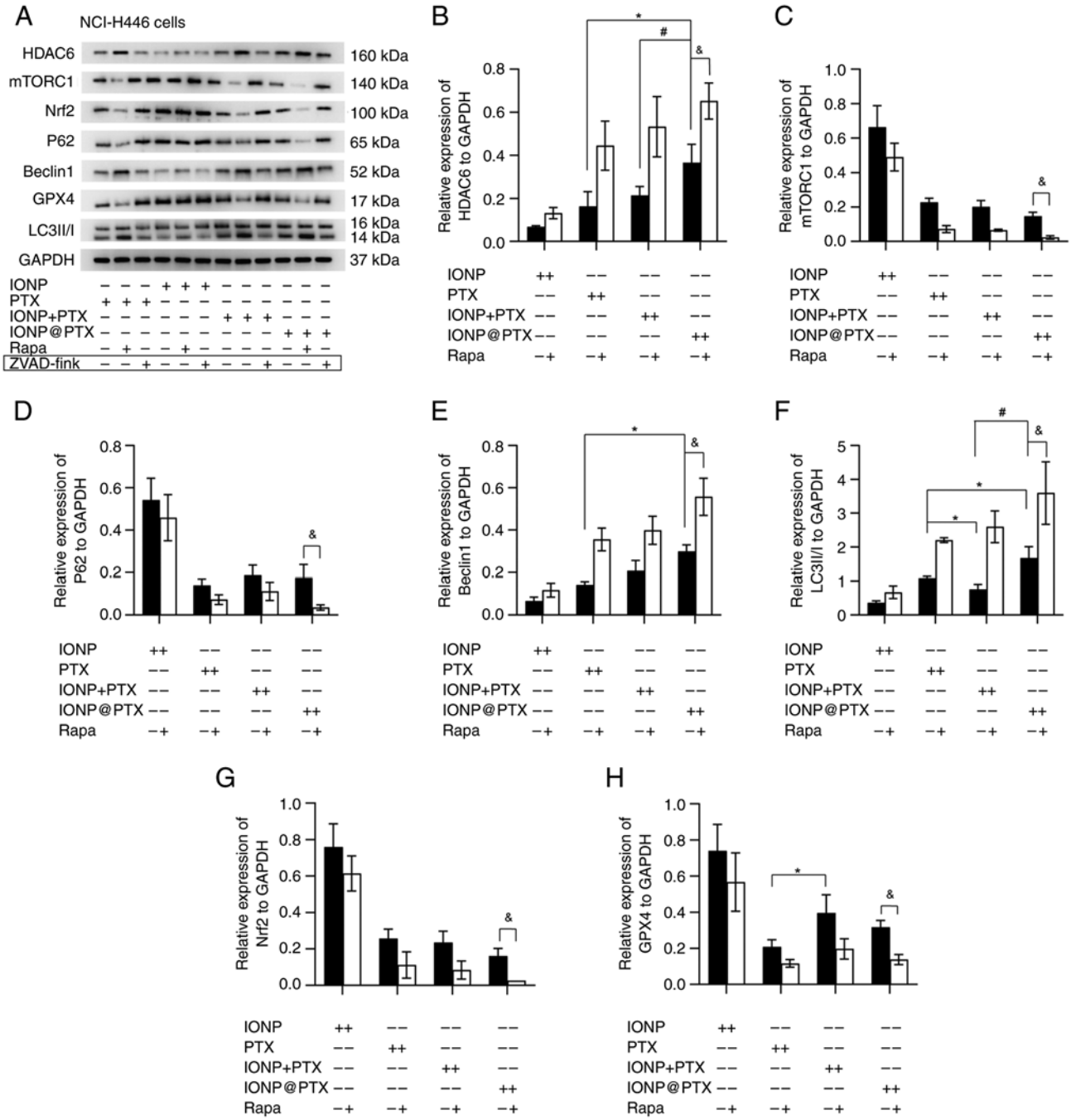

Figure 3. Effects of IONP@PTX on the expression of ferroptosis-related proteins and autophagy-related proteins in NCI-H446 cells. (A) Representative western blot analysis of ferroptosis-related proteins and autophagy-related proteins in NCI-H446 cells following treatment with different drugs for 24 h. (B-F) Relative expression of autophagy-related proteins HDAC6, mTORC1, p62, Beclin 1 and LC3-II/I in NCI-H446 cells following treatment with or without 50 nmol/l rapamycin for 24 h. *P<0.05 vs. PTX group. #P<0.05 vs. IONP + PTX group; &P<0.05 vs. IONP@PTX monotherapy (without rapamycin) group. (G) Relative expression of ferroptosis-related protein Nrf2 in NCI-H446 cells following treatment with or without 50 nmol/l rapamycin for 24 h. (H) Relative expression of ferroptosis-related protein GPX4 in NCI-H446 cells following treatment with or without 50 nmol/l rapamycin for 24 h. *P<0.05 vs. PTX group (without rapamycin). &P<0.05 vs. IONP@PTX monotherapy (without rapamycin). Data were obtained from three independent repeated experiments. In the western blot analysis, the IONP group was used as the control group due to the large loading of IONP samples, which had lower toxicity on NCI-H446 cells. The results of the circled strips are not reflected in this article. IONP, iron oxide nanoparticles; PTX, paclitaxel; Nrf2, nuclear factor erythrocyte 2 related factor 2; GPX4, glutathione peroxidase 4; p62, sequestosome1; Rapa, rapamycin.

However, it is not clear whether the observed effect was produced by bundling IONP with PTX to form a compound drug or by only simply adding nanoparticles with PTX. Unlike the nanoparticles used to induce ferroptosis investigated in our previous studies, the IONP@PTX used in the present study is a composite drug formed by bundling nanoparticles with the antitumor drug PTX. Considering that brain metastasis of lung cancer is one of the most common distant metastatic sites (60), the present authors chose two tumor cell lines (NCI-H446 and M059K) that differ from the ones used in our previous study (U251 and HMC3) to investigate the possible antitumor effect. The experimental results have demonstrated that PTX has a

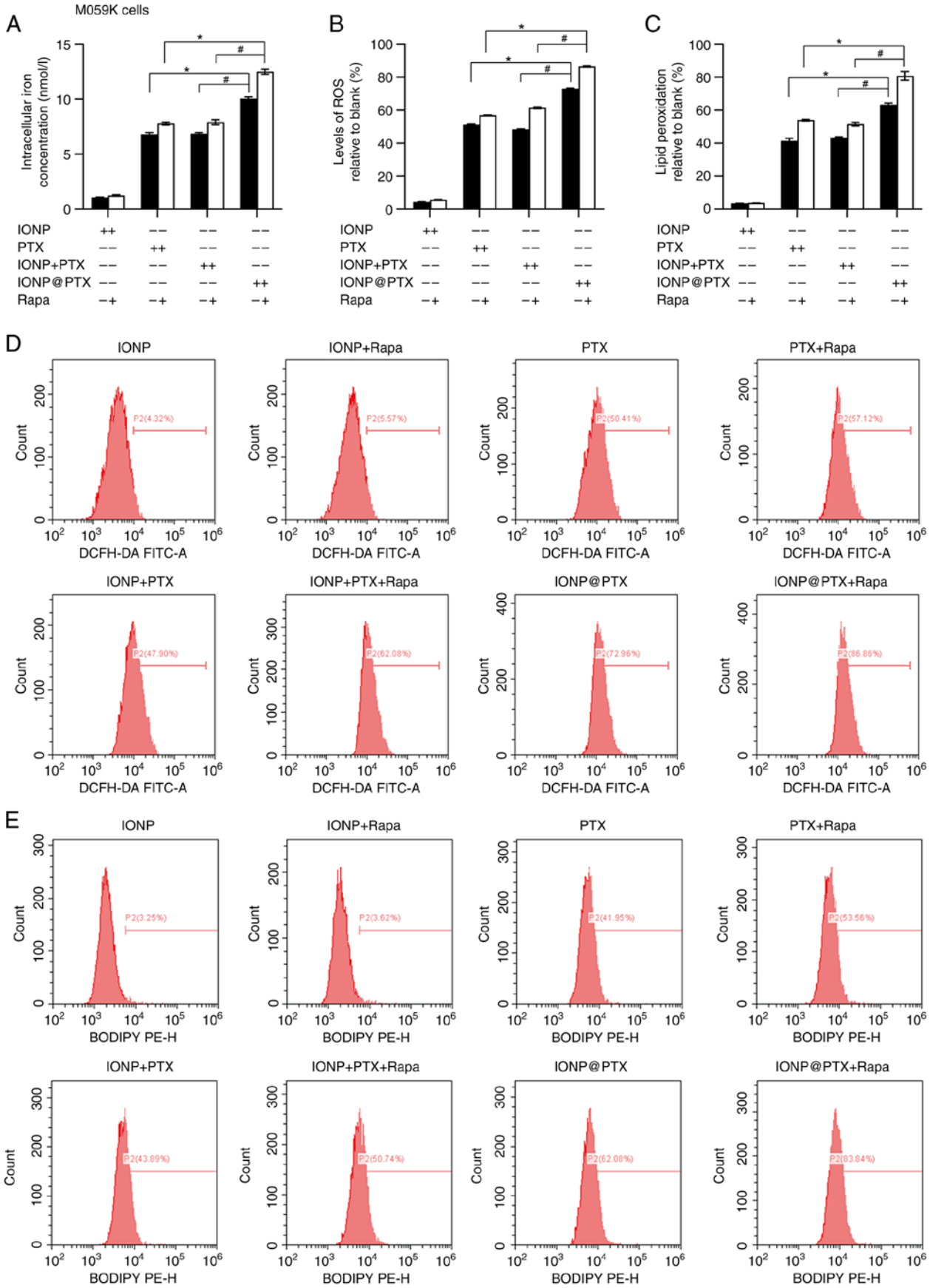

Figure 4. Changes in biochemical indices related to ferroptosis in M059K cells following IONP@PTX treatment. (A) Intracellular iron concentration in M059K cells following treatment with or without 50 nmol/l rapamycin for 24 h. (B) Relative levels of ROS in M059K cells following treatment with or without 50 nmol/l rapamycin for 24 h. (C) Relative levels of lipid peroxidation in M059K cells following treatment with or without 50 nmol/l rapamycin for 24 h. (D) Flow cytometry analysis using DCFH-DA fluorescent probe to measure intracellular ROS content. (E) Flow cytometry analysis using C11-BODIPY fluorescent probe to detect intracellular lipid peroxidation content. *P<0.05 vs. the PTX group; #P<0.05 vs. IONP + PTX group. Data were obtained from three independent repeated experiments. IONP, iron oxide nanoparticles; PTX, paclitaxel; ROS, reactive oxygen species.

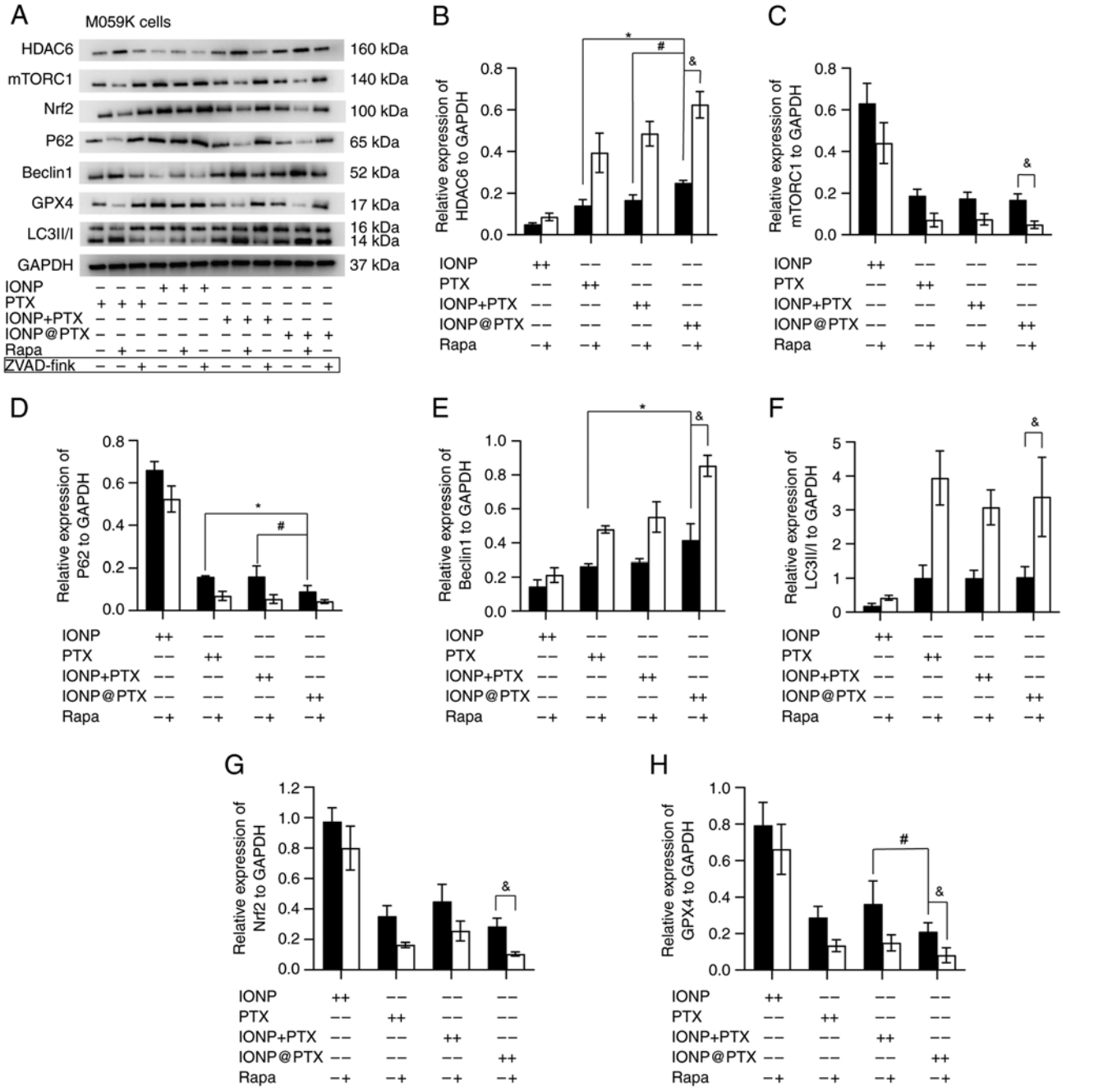

Figure 5. Effects of IONP@PTX on the expression of ferroptosis-related proteins and autophagy-related proteins in M059K cells. (A) Representative western blot analysis of ferroptosis-related proteins and autophagy-related proteins in M059K cells following treatment with different drugs for 24 h. (B-F) Relative expression of autophagy-related proteins HDAC6, mTORC1, p62, Beclin1 and LC3-II/I in the M059K cells following treatment with or without 50 nmol/l rapamycin for 24 h. *P<0.05 vs. PTX group. $^{\#}$P<0.05, vs. IONP + PTX group. $^{\&}$P<0.05, vs. IONP@PTX (without rapamycin) group. (G) Relative expression of ferroptosis-related protein Nrf2 in M059K cells following treatment with or without 50 nmol/l rapamycin for 24 h. (H) The relative expression of ferroptosis-related protein GPX4 in M059K cells following treatment with or without 50 nmol/l rapamycin for 24 h. $^{\#}$P<0.05 vs. IONP + PTX group. $^{\&}$P<0.05 vs. IONP@PTX (no rapamycin) group. Data were obtained from three independent repeated experiments. In the western blot analysis, the IONP group was used as the control group due to the large loading of IONP samples, which had lower toxicity in M059K cells. The results of the circled strips are not reflected in this article. IONP, iron oxide nanoparticles; PTX, paclitaxel; Nrf2, nuclear factor erythrocyte 2 related factor 2; GPX4, glutathione peroxidase 4; HDAC6, histone deacetylase 6; mTORC1, mammalian target of rapamycin complex 1; LC3, light chain 3; p62, sequestosome1; Rapa, rapamycin.

certain inhibitory effect on viability in NCI-H446 and M059K cells, whereas IONP monotherapy does not. Notably, the combination index of the IONP + PTX was between 0.85-1.15 and that of IONP@PTX was >1.15 in NCI-H446 and M059K cells, implying that IONP@PTX produces a synergistic effect in different types of intracranial tumors, such as primary and secondary brain tumors, and the synergistic effect of IONP@PTX is not a coincidence. Accordingly, IONP@PTX could be used in different kinds of brain tumors, laying the foundation for subsequent application-based studies.

Ferroptosis is usually accompanied by massive iron accumulation and iron-dependent LPD (61). The GPX family was shown to be capable of breaking down aberrant endogenous peroxides, among which GPX4 is the only enzyme that can

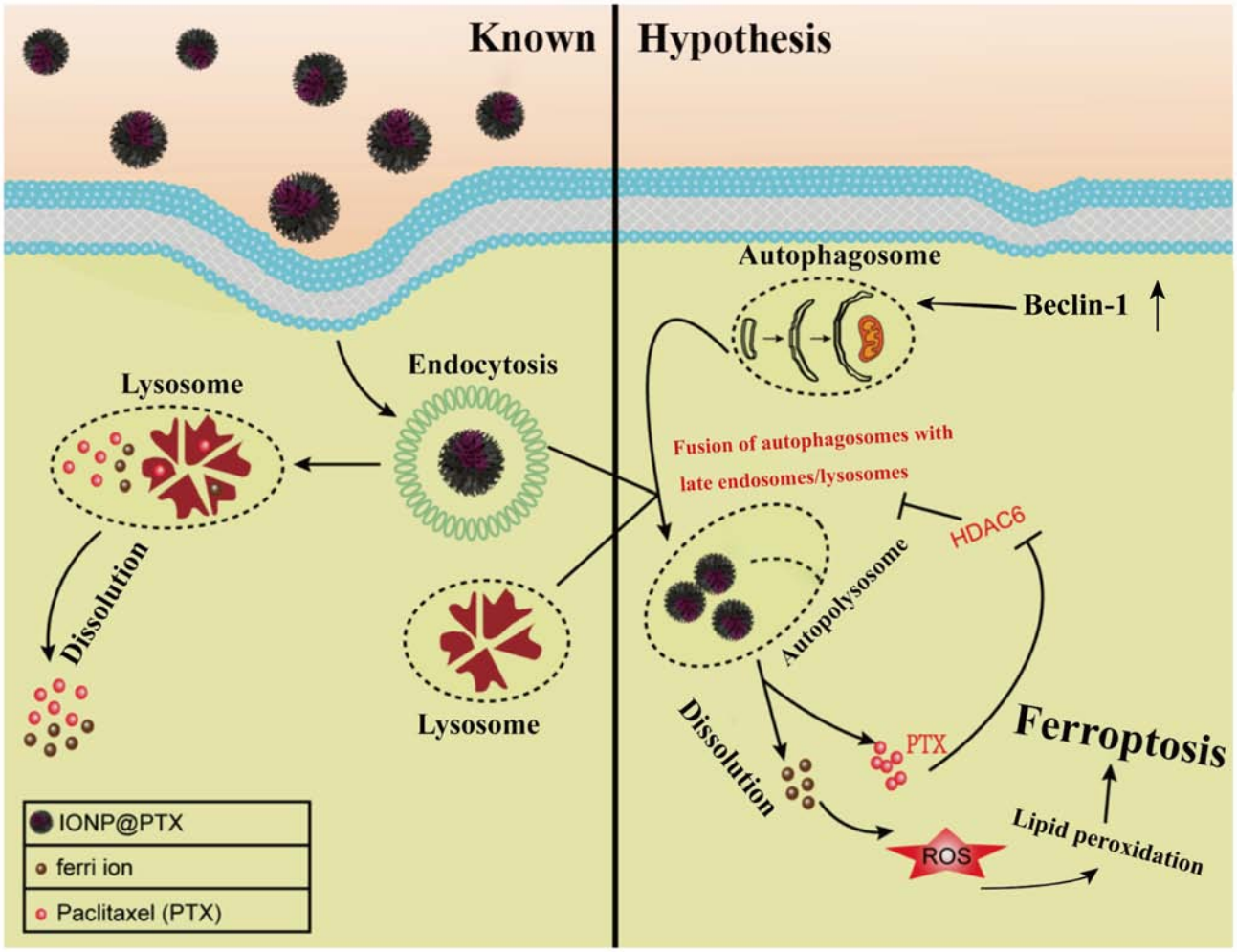

Figure 6. Proposed schematic diagram of the IONP@PTX mode of action. IONP, iron oxide nanoparticles; PTX, paclitaxel; ROS, reactive oxygen species; HDAC6, recombinant histone deacetylase 6.

reduce lipid membrane peroxides and its inactivation is central in ferroptosis (62). In turn, GSH is a key cofactor for the selenoprotein GPX4. When intracellular GSH levels fall, GPX4 activity decreases and intracellular ROS and lipid peroxide accumulation increases, eventually leading to cellular ferroptosis (46). Nrf2 is a basic leucine zipper transcription factor that participates in antioxidant reduction processes, lipid metabolism control and iron metabolism (47). The present study found that IONP@PTX substantially raised total iron ion concentration, ROS, and LPD levels in NCI-H446 and M059K cells when compared with PTX or PTX + IONP. This finding was similar to that of our previous investigation on GBM U251 cells (32). Using malignant GBM M059K cells *in vitro*, the present study confirmed that IONP@PTX significantly decreased the expression of ferroptosis-related GPX4 protein compared with the IONP + PTX, but the expression levels of Nrf2 and GPX4 were not significantly reduced in other groups. It can be inferred that the IONP@PTX-induced ferroptosis does not occur through the normal Nrf2 and GPX4 routes, most likely due to the cells' heightened sensitivity to ferroptosis caused by GSH depletion. We hypothesized that IONP@PTX significantly increased total iron ion concentration and abnormal labile iron pools, thus making cells more vulnerable to ferroptosis (63-66). Although IONP@PTX did not reduce Nrf2 and GPX4 levels, it caused a significant increase in ROS and LPD accumulation in both cell lines. The main reason for this is that the increased intracellular GSH demand is insufficient to support the effective elimination of phospholipid hydroperoxides, eventually resulting in ferroptosis (67). Notably, the IONP@PTX + rapamycin can release more iron ions, causing LPD and ferroptosis in NCI-H446 and M059K cells. These findings imply that IONP@PTX-induced ferroptosis may be associated with autophagy.

Recently, the relationship between autophagy and cancer has attracted considerable attention (68). Autophagy is a defense mechanism that maintains cellular homeostasis and promotes cell survival by eliminating damaged organelles or abnormal proteins; it is also a lysosome-mediated degradation pathway (69) that affects all stages of tumor initiation and progression (68,70,71). Microtubule-associated proteins LC3, mTOR, Beclin 1 and p62 are central autophagy-related genes involved in the regulation of the autophagic process (72). Among them, Beclin 1 and LC3 mainly regulate autophagosome formation (73), while p62 is an effector of selective autophagy as well as a substrate of nuclear autophagy (73,74). A recent study has documented that rapamycin, a mTORC1 receptor-specific inhibitor, can

regulate the mTOR pathway to activate autophagy (71). It is known that at the core of the autophagy process is the conversion from LC3-I to LC3-II, and the expression of LC3-II has been shown to be a marker of autophagic activity, therefore the expression of the LC3-II/I ratio can be used to evaluate the level of autophagy (75). The present results showed that IONP@PTX increased the level of LC3-II/I and decreased that of mTORC1 in NCI-H446 cells. Moreover, additional rapamycin enhanced the IONP@PTX-induced upregulation of LC3 and downregulation of mTORC1 in both cell lines. IONP@PTX did not significantly increase the expression level of LC3 but it showed a significant increase in the conversion from LC3-I to LC3-II in M095K cells. In our previous study, it was documented that, compared with PTX monotherapy, IONP@PTX significantly increased the expression of LC3 protein in glioma U251 cells (32). Accumulating evidence has indicated that PTX plays a vital role in antagonizing the production of HDAC6 protein (76-78). The detection of autophagy-related proteins in the present study revealed that only the expression of autophagy-related proteins HDAC6 and Beclin1 jointly increased in H446 and M059K cells, without marked changes in other indicators. Notably, additional rapamycin enhanced IONP@PTX-induced upregulation of Beclin1 and HDAC6 in both cell lines. These results suggest that IONP@PTX induces a synergistic effect on cellular ferroptosis, most likely, through the autophagy pathway. Based on the above findings, it is hypothesized for the role of IONP@PTX, that is, IONP@PTX synergistically induces cellular ferroptosis by affecting the Beclin1-HDAC6 autophagic pathway. Specifically, IONP@PTX enhances autophagy and increases autophagosome formation by upregulating Beclin1 after endocytosis and induces ferroptosis by promoting the recruitment of HDAC6 to facilitate the fusion of autophagosomes with late endosomes/lysosomes. In turn, HDAC6 acetylates microtubulin to destabilize it and inhibits autophagosome-lysosome fusion, thereby creating a feedback inhibition loop between autophagosome-lysosome fusion and HDAC6, and inhibiting IONP@PTX degradation. Once the balance is disturbed, the autophagic degradation results in a continuous degradation of IONP@PTX, subsequently releasing PTX and iron ions. The PTX released from the IONP@PTX complex following endocytosis antagonizes this feedback inhibition loop of HDAC6, thus breaking this balance and promoting autophagosome-lysosome fusion. On the other hand, the released PTX and iron ions synergistically promoted ferroptosis, ultimately producing a significant and enhanced synergistic induction of ferroptosis compared with PTX monotherapy or IONP + PTX (Fig. 6). Further studies are required to test the validity of this hypothesis. In the following study, tumor models will be created using NCI-H446 (or M059K) cells in nude mice to further investigate whether IONP@PTX can synergistically induce ferroptosis through the autophagic pathway *in vivo*. Subsequently, Beclin1 and HDAC6 knocked down or overexpressing nude mice models will be created to verify the effects and key roles of these two genes in the synergistic effect of IONP@PTX in inducing ferroptosis through autophagy. In addition, the effect of IONP@PTX on the capacity of migrate, invade and apoptosis should be further studied in NCI-H446 and M059K cell lines.

In conclusion, IONP bundled with PTX exerts a synergistic effect on the viability of NCI-H446 and M059K cell lines by inducing cellular ferroptosis, which may be associated with autophagy.

Acknowledgements

Not applicable.

Funding

This work was supported by the National Natural Science Foundation of China (grant no. 32060228), the Guangxi Natural Science Foundation Project (grant nos. 2023GXNSFAA026385, 2022JJA140211, 2017GXNSFAA198112 and 2019GXNSFAA245077), Research and Innovation Base for Basic and Clinical Application of Nerve Injury and Repair (grant no. ZY21195042), Guangxi Key Laboratory of Big Data Intelligent Cloud Management for Neurological Diseases (grant no. ZTJ2020005) and Guilin Scientific Research and Technology Development Project (grant no. 20190219-2).

Availability of data and materials

The datasets used and/or analyzed during the current study are available from the corresponding author on reasonable request.

Authors' contributions

QN was responsible for conceptualization, subject design, experimental framework construction and *in vitro* experiments, and was a major contributor in writing the manuscript. WC performed *in vitro* experiments, western blotting, data analysis and management, and draft revision. TZ assisted with the experimental design, *in vitro* experiments, data analysis and literature review. SY was responsible for data analysis, statistical analysis, design research, literature search and collation. ZR helped with the experimental approach, and the concept and design of the study. PZ was responsible for assisting in the design of experimental methods and the production of manuscript images. JW was responsible for methodology, project funding acquisition, manuscript framework design, experimental supervision and critical revision of important intellectual content. QN and WC confirm the authenticity of all the raw data. All authors read and approved the final version of the manuscript.

Ethics approval and consent to participate

Not applicable.

Patient consent for publication

Not applicable.

Competing interests

The authors declare that they have no competing interests.

References

1. Thai AA, Solomon BJ, Sequist LV, Gainor JF and Heist RS: Lung cancer. Lancet 398: 535-554, 2021.
2. Xia C, Dong X, Li H, Cao M, Sun D, He S, Yang F, Yan X, Zhang S, Li N and Chen W: Cancer statistics in China and United States, 2022: Profiles, trends, and determinants. Chin Med J (Engl) 135: 584-590, 2022.
3. Caeser R, Egger JV, Chavan S, Socci ND, Jones CB, Kombak FE, Asher M, Roehrl MH, Shah NS, Allaj V, *et al*: Genomic and transcriptomic analysis of a library of small cell lung cancer patient-derived xenografts. Nat Commun 13: 2144, 2022.
4. Siegel RL, Miller KD and Jemal A: Cancer statistics, 2018. CA Cancer J Clin 68: 7-30, 2018.
5. Yuan M, Zhao Y, Arkenau HT, Lao T, Chu L and Xu Q: Signal pathways and precision therapy of small-cell lung cancer. Signal Transduct Target Ther 7: 187, 2022.
6. Mak DWS, Li S and Minchom A: Challenging the recalcitrant disease-developing molecularly driven treatments for small cell lung cancer. Eur J Cancer 119: 132-150, 2019.
7. George J, Lim JS, Jang SJ, Cun Y, Ozretić L, Kong G, Leenders F, Lu X, Fernández-Cuesta L, Bosco G, *et al*: Comprehensive genomic profiles of small cell lung cancer. Nature 524: 47-53, 2015.
8. Low JT, Ostrom QT, Cioffi G, Neff C, Waite KA, Kruchko C and Barnholtz-Sloan JS: Primary brain and other central nervous system tumors in the United States (2014-2018): A summary of the CBTRUS statistical report for clinicians. Neurooncol Pract 9: 165-182, 2022.
9. Lapointe S, Perry A and Butowski NA: Primary brain tumours in adults. Lancet 392: 432-446, 2018.
10. Zhou YS, Wang W, Chen N, Wang LC and Huang JB: Research progress of anti-glioma chemotherapeutic drugs (review). Oncol Rep 47: 101, 2022.
11. Tan AC, Ashley DM, López GY, Malinzak M, Friedman HS and Khasraw M: Management of glioblastoma: State of the art and future directions. CA Cancer J Clin 70: 299-312, 2020.
12. Zhang Y, Zhai M, Chen Z, Han X, Yu F, Li Z, Xie X, Han C, Yu L, Yang Y and Mei X: Dual-modified liposome codelivery of doxorubicin and vincristine improve targeting and therapeutic efficacy of glioma. Drug Deliv 24: 1045-1055, 2017.
13. d'Angelo M, Castelli V, Benedetti E, Antonosante A, Catanesi M, Dominguez-Benot R, Pitari G, Ippoliti R and Cimini A: Theranostic nanomedicine for malignant gliomas. Front Bioeng Biotechnol 7: 325, 2019.
14. Zhu L and Chen L: Progress in research on paclitaxel and tumor immunotherapy. Cell Mol Biol Lett 24: 40, 2019.
15. Zeng W, Kwan Law BY, Wai Wong VK, Bik Chan DS, Fai Mok SW, Ying Gao JJ, Yan Ho RK, Liang X, Li JH, Lee MT, *et al*: HM30181A, a potent P-glycoprotein inhibitor, potentiates the absorption and in vivo antitumor efficacy of paclitaxel in an orthotopic brain tumor model. Cancer Biol Med 17: 986, 2020.
16. Yang YH, Mao JW and Tan XL: Research progress on the source, production, and anti-cancer mechanisms of paclitaxel. Chin J Nat Med 18: 890-897, 2020.
17. Gonzalez-Angulo AM and Hortobagyi GN: Optimal schedule of paclitaxel: Weekly is better. J Clin Oncol 26: 1585-1587, 2008.
18. Joos G, Schallier D, Pinson P, Sterckx M and Van Meerbeeck JP: Paclitaxel (PTX) as second line treatment in patients (pts) with small cell lung cancer (SCLC) refractory to carboplatin-etoposide: A multicenter phase II study. J Clin Oncol 22 (14 Suppl): S7211, 2004.
19. Nakao M, Fujita K, Suzuki Y, Arakawa S, Sakai Y, Sato H and Muramatsu H: Nab-paclitaxel monotherapy for relapsed small cell lung cancer: Retrospective analysis and review. Anticancer Res 40: 1579-1585, 2020.
20. Ahmed Khalil A, Rauf A, Alhumaydhi FA, Aljohani ASM, Javed MS, Khan MA, Khan IA, El-Esawi MA, Bawazeer S, Bouyahya A, *et al*: Recent developments and anticancer therapeutics of paclitaxel: An update. Curr Pharm Des 28: 3363-3373, 2022.
21. Silva P, Nascimento A, Martinho O, Reis R and Bousbaa H: Targeting BUB3 in combination with paclitaxel inhibits proliferation of glioblastoma cells by enhancing cellular senescence. Sci Lett 1: 1, 2022.
22. Erthal LCS, Shi Y, Sweeney KJ, Gobbo OL and Ruiz-Hernandez E: Nanocomposite formulation for a sustained release of free drug and drug-loaded responsive nanoparticles: An approach for a local therapy of glioblastoma multiforme. Sci Rep 13: 5094, 2023.
23. Wu HC, Feng Y, Song XY, Song CY, Chen JL, Wang YC, He XL, Liang RC, Li JH and Tan H: Implantable polyurethane scaffolds loading with PEG-paclitaxel conjugates for the treatment of glioblastoma multiforme. Chin J Polym Sci 40: 491-503, 2022.
24. Jibodh RA, Lagas JS, Nuijen B, Beijnen JH and Schellens JH: Taxanes: Old drugs, new oral formulations. Eur J Pharmacol 717: 40-46, 2013.
25. Sharifi-Rad J, Quispe C, Patra JK, Singh YD, Panda MK, Das G, Adetunji CO, Michael OS, Sytar O, Polito L, *et al*: Paclitaxel: Application in modern oncology and nanomedicine-based cancer therapy. Oxid Med Cell Longev 2021: 3687700, 2021.
26. Mali P and Sherje AP: Cellulose nanocrystals: Fundamentals and biomedical applications. Carbohydr Polym 275: 118668, 2022.
27. Kahn B, Collazo J and Kyprianou N: Androgen receptor as a driver of therapeutic resistance in advanced prostate cancer. Int J Biol Sci 10: 588-595, 2014.
28. Li K, Zhan W, Chen Y, Jha RK and Chen X: Docetaxel and doxorubicin codelivery by nanocarriers for synergistic treatment of prostate cancer. Front Pharmacol 10: 1436, 2019.
29. Pulvirenti L, Monforte F, Lo Presti F, Li Volti G, Carota G, Sinatra F, Bongiorno C, Mannino G, Cambria MT and Condorelli GG: Synthesis of MIL-modified Fe_3O_4 magnetic nanoparticles for enhancing uptake and efficiency of temozolomide in glioblastoma treatment. Int J Mol Sci 23: 2874, 2022.
30. Fernández-Acosta R, Iriarte-Mesa C, Alvarez-Alminaque D, Hassannia B, Wiernicki B, Díaz-García AM, Vandenabeele P, Vanden Berghe T and Pardo Andreu GL: Novel iron oxide nanoparticles induce ferroptosis in a panel of cancer cell lines. Molecules 27: 3970, 2022.
31. Xu Y, Wu H, Huang J, Qian W, Martinson DE, Ji B, Li Y, Wang YA, Yang L and Mao H: Probing and enhancing ligand-mediated active targeting of tumors using sub-5 nm ultrafine iron oxide nanoparticles. Theranostics 10: 2479-2494, 2020.
32. Chen H and Wen J: Iron oxide nanoparticles loaded with paclitaxel inhibits glioblastoma by enhancing autophagy-dependent ferroptosis pathway. Eur J Pharmacol 921: 174860, 2022.
33. Rakesh R, PriyaDharshini LC, Sakthivel KM and Rasmi RR: Role and regulation of autophagy in cancer. Biochim Biophys Acta Mol Basis Dis 1868: 166400, 2022.
34. Ma Q, Long S, Gan Z, Tettamanti G, Li K and Tian L: Transcriptional and post-transcriptional regulation of autophagy. Cells 11: 441, 2022.
35. Li X, Yang KB, Chen W, Mai J, Wu XQ, Sun T, Wu RY, Jiao L, Li DD, Ji J, *et al*: CUL3 (cullin 3)-mediated ubiquitination and degradation of BECN1 (beclin 1) inhibit autophagy and promote tumor progression. Autophagy 17: 4323-4340, 2021.
36. Ciołczyk-Wierzbicka D, Krawczyk A, Zarzycka M, Zemanek G and Wierzbicki K: Three generations of mTOR kinase inhibitors in the activation of the apoptosis process in melanoma cells. J Cell Commun Signal 17: 975-989, 2023.
37. Zou Z, Tao T, Li H and Zhu X: mTOR signaling pathway and mTOR inhibitors in cancer: Progress and challenges. Cell Biosci 10: 31, 2020.
38. Zhang L, Fang Y, Cheng X, Lian Y and Xu H: Interaction between TRPML1 and p62 in regulating autophagosome-lysosome fusion and impeding neuroaxonal dystrophy in Alzheimer's disease. Oxid Med Cell Longev 2022: 8096009, 2022.
39. Hai R, Yang D, Zheng F, Wang W, Han X, Bode AM and Luo X: The emerging roles of HDACs and their therapeutic implications in cancer. Eur J Pharmacol 931: 175216, 2022.
40. Tang Q, Li X and Wang J: Tubulin deacetylase NDST3 modulates lysosomal acidification: Implications in neurological diseases. Bioessays 44: e2200110, 2022.
41. Li J, Yu M, Fu S, Liu D and Tan Y: Role of selective histone deacetylase 6 inhibitor ACY-1215 in cancer and other human diseases. Front Pharmacol 13: 907981, 2022.
42. Johansen T and Lamark T: Selective autophagy: ATG8 family proteins, LIR motifs and cargo receptors. J Mol Biol 432: 80-103, 2020.
43. Zhou B, Liu J, Kang R, Klionsky DJ, Kroemer G and Tang D: Ferroptosis is a type of autophagy-dependent cell death. Semin Cancer Biol 66: 89-100, 2020.
44. Zhang X, Ge H, Ma Y, Song L, Ma Y, Tian G, Wang L, Meng Q and Sun X: Engineered anti-cancer nanomedicine for synergistic ferroptosis-immunotherapy. Chem Eng J 455: 140688, 2023.
45. Shen Z, Liu T, Li Y, Lau J, Yang Z, Fan W, Zhou Z, Shi C, Ke C, Bregadze VI, *et al*: Fenton-reaction-acceleratable magnetic nanoparticles for ferroptosis therapy of orthotopic brain tumors. ACS Nano 12: 11355-11365, 2018.

46. Stockwell BR: Ferroptosis turns 10: Emerging mechanisms, physiological functions, and therapeutic applications. Cell 185: 2401-2421, 2022.
47. Song X and Long D: Nrf2 and ferroptosis: A new research direction for neurodegenerative diseases. Front Neurosci 14: 267, 2020.
48. Mouri A, Yamaguchi O, Miyauchi S, Shiono A, Utsugi H, Nishihara F, Murayama Y, Kagamu H and Kobayashi K: Combination therapy with carboplatin and paclitaxel for small cell lung cancer. Respir Investig 57: 34-39, 2019.
49. Yun T, Kim HT, Han JY, Yoon SJ, Kim HY, Nam BH and Lee JS: A phase II study of weekly paclitaxel plus gemcitabine as a second-line therapy in patients with metastatic or recurrent small cell lung cancer. Cancer Res Treat 48: 465-472, 2016.
50. Oi H, Matsuda T, Kimura T, Morise M, Yamano Y, Yokoyama T, Kataoka K and Kondoh Y: Weekly nanoparticle albumin-bound paclitaxel and paclitaxel for relapsed small cell lung cancer: A retrospective observational study. Medicine (Baltimore) 101: e28863, 2022.
51. Mittal S, Ali J and Baboota S: Overcoming the challenges in the treatment of glioblastoma via nanocarrier-based drug delivery approach. Curr Pharm Des 27: 4539-4556, 2021.
52. Wang L, Wang X, Shen L, Alrobaian M, Panda SK, Almasmoum HA, Ghaith MM, Almaimani RA, Ibrahim IAA, Singh T, *et al*: Paclitaxel and naringenin-loaded solid lipid nanoparticles surface modified with cyclic peptides with improved tumor targeting ability in glioblastoma multiforme. Biomed Pharmacother 138: 111461, 2021.
53. Zhang DY, Dmello C, Chen L, Arrieta VA, Gonzalez-Buendia E, Kane JR, Magnusson LP, Baran A, James CD, Horbinski C, *et al*: Ultrasound-mediated delivery of paclitaxel for glioma: A comparative study of distribution, toxicity, and efficacy of albumin-bound versus cremophor formulations. Clin Cancer Res 26: 477-486, 2020.
54. Liu W, Lin Q, Fu Y, Huang S, Guo C, Li L, Wang L, Zhang Z and Zhang L: Target delivering paclitaxel by ferritin heavy chain nanocages for glioma treatment. J Control Release 323: 191-202, 2020.
55. Chen T, Gong T, Zhao T, Liu X, Fu Y, Zhang Z and Gong T: Paclitaxel loaded phospholipid-based gel as a drug delivery system for local treatment of glioma. Int J Pharm 528: 127-132, 2017.
56. Wang X, Ye L, He W, Teng C, Sun S, Lu H, Li S, Lv L, Cao X, Yin H, *et al*: In situ targeting nanoparticles-hydrogel hybrid system for combined chemo-immunotherapy of glioma. J Control Release 345: 786-797, 2022.
57. Que W, Li S and Chen J: NS-398 enhances the efficacy of bortezomib against RPMI8226 human multiple myeloma cells. Mol Med Rep 7: 1641-1645, 2013.
58. Wen J, Chen H, Ren Z, Zhang P, Chen J and Jiang S: Ultrasmall iron oxide nanoparticles induced ferroptosis via Beclin1/ATG5-dependent autophagy pathway. Nano Converg 8: 10, 2021.
59. Sugiyama A, Ohta T, Obata M, Takahashi K, Seino M and Nagase S: xCT inhibitor sulfasalazine depletes paclitaxel-resistant tumor cells through ferroptosis in uterine serous carcinoma. Oncol Lett 20: 2689-2700, 2020.
60. Rudin CM, Brambilla E, Faivre-Finn C and Sage J: Small-cell lung cancer. Nat Rev Dis Primers 7: 3,2021.
61. Li J, Cao F, Yin HL, Huang ZJ, Lin ZT, Mao N, Sun B and Wang G: Ferroptosis: Past, present and future. Cell Death Dis 11: 88, 2020.
62. Chang S, Tang M, Zhang B, Xiang D and Li F: Ferroptosis in inflammatory arthritis: A promising future. Front Immunol 13: 955069, 2022.
63. He H, Du L, Guo H, An Y, Lu L, Chen Y, Wang Y, Zhong H, Shen J, Wu J and Shuai X: Redox responsive metal organic framework nanoparticles induces ferroptosis for cancer therapy. Small 16: 2001251, 2020.
64. Xue CC, Li MH, Zhao Y, Zhou J, Hu Y, Cai KY, Zhao Y, Yu SH and Luo Z: Tumor microenvironment-activatable Fe-doxorubicin preloaded amorphous $CaCO_3$ nanoformulation triggers ferroptosis in target tumor cells. Sci Adv 6: eaax1346, 2020.
65. Chen G, Yang Y, Xu Q, Ling M, Lin H, Ma W, Sun R, Xu Y, Liu X, Li N, *et al*: Self-amplification of tumor oxidative stress with degradable metallic complexes for synergistic cascade tumor therapy. Nano Lett 20: 8141-8150, 2020.
66. Luo S, Ma D, Wei R, Yao W, Pang X, Wang Y, Xu X, Wei X, Guo Y, Jiang X, *et al*: A tumor microenvironment responsive nanoplatform with oxidative stress amplification for effective MRI-based visual tumor ferroptosis. Acta Biomater 138: 518-527, 2022.
67. Friedmann Angeli JP, Krysko DV and Conrad M: Ferroptosis at the crossroads of cancer-acquired drug resistance and immune evasion. Nat Rev Cancer 19: 405-414, 2019.
68. Assi M and Kimmelman AC: Impact of context-dependent autophagy states on tumor progression. Nat Cancer 4: 596-607, 2023.
69. Zhang X, Sui S, Wang L, Li H, Zhang L, Xu S and Zheng X: Inhibition of tumor propellant glutathione peroxidase 4 induces ferroptosis in cancer cells and enhances anticancer effect of cisplatin. J Cell Physiol 235: 3425-3437, 2020.
70. Xia H, Green DR and Zou W: Autophagy in tumour immunity and therapy. Nat Rev Cancer 21: 281-297, 2021.
71. Yang F, Du L, Song G, Zong X, Jin X, Yang X and Qi Z: Rapamycin and 3-methyladenine influence the apoptosis, senescence, and adipogenesis of human adipose-derived stem cells by promoting and inhibiting autophagy: An in vitro and in vivo study. Aesthetic Plast Surg 45: 1294-1309, 2021.
72. Ding R, Liu Z, Tan J and Sun B: Advanced oxidation protein products mediate human keratinocytes apoptosis by inducing cell autophagy through the mTOR-Beclin-1 pathway. Cell Biochem Funct 40: 880-887, 2022.
73. Rhaman A, Mahmoud E, Abu Alfadl EM, Mohammed DH and Sheneef A: Expression of autophagy related genes mTOR, ATG10 and P62 in the peripheral blood mononuclear cells of systemic lupus erythematosus Egyptian patients. Egypt J Med Microbiol 32: 133-140, 2023.
74. Zhang J, Han L, Ma Q, Wang X, Yu J, Xu Y, Zhang X, Wu X and Deng G: RIP3 impedes Mycobacterium tuberculosis survival and promotes p62-mediated autophagy. Int Immunopharmacol 115: 109696, 2023.
75. Schaaf MBE, Keulers TG, Vooijs MA and Rouschop KMA: LC3/GABARAP family proteins: Autophagy-(un) related functions. FASEB J 30: 3961-3978, 2016.
76. Gordon MS, Shapiro GI, Sarantopoulos J, Juric D, Lu B, Zarotiadou A, Connarn JN, Le Bruchec Y, Dumitru CD and Harvey RD: Phase Ib study of the histone deacetylase 6 inhibitor citarinostat in combination with paclitaxel in patients with advanced solid tumors. Front Oncol 11: 786120, 2022.
77. Zhang N, Sun P, Jin H, Yang Y, Zhao Q, Zhou L, Guo L, Yang X and Lu L: Chidamide combined with paclitaxel effectively reverses the expression of histone deacetylase in lung cancer. Anticancer Drugs 31: 702-708, 2020.
78. Yoo J, Jeon YH, Lee DH, Kim GW, Lee SW, Kim SY, Park J and Kwon SH: HDAC6-selective inhibitors enhance anticancer effects of paclitaxel in ovarian cancer cells. Oncol Lett 21: 201, 2021.